

Phosphino-Aminothiazoline Platinum(II) and Platinum(II)/Gold(I) Complexes: Structural, Chemical and Vapoluminescent Properties

Roberto Pattacini,^[a] Carlo Giansante,^[b] Paola Ceroni,^{*[b]} Mauro Maestri,^[b] and Pierre Braunstein^{*[a]}

Dedicated to Prof. G. van Koten on the occasion of his 65th birthday

Abstract: Phosphino-amino-thiazolines and -thiazoles can exist in solution in two tautomeric forms, in which the N–H proton involves the endo-cyclic or exo-cyclic nitrogen atom. The two tautomers show different reactivities toward alcoholysis; the imino form degrades more rapidly. Their bischelated platinum complexes were studied in the solid state by single crystal X-ray diffraction. Thus, the unique stereo-

electronic features of the [Pt(PN_{th})₂] (PN_{th} = diphenylphosphino-aminothiazoline) moiety were revealed. The complex *cis*-[Pt(PN_{th})₂] reacts with gold(I) salts to yield dimetallic compounds, the

molecular structures of which have been determined by X-ray diffraction. Solid *cis*-[Pt(PN_{th})₂] shows vapoluminescent properties if exposed to alcohol vapors. A combined photophysical and crystallographic investigation has been carried out to clarify the unprecedented rigidochromic role of the alcohol in this phenomenon.

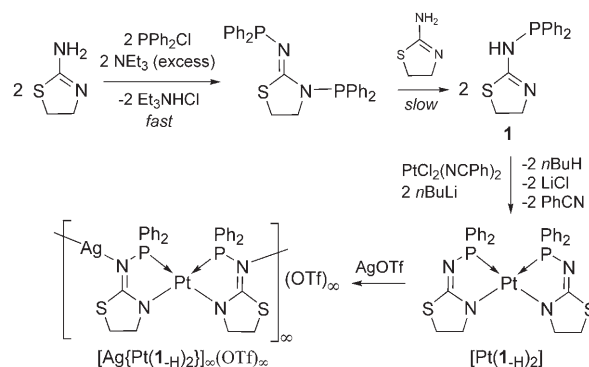
Keywords: dimetallic complexes • luminescence • metalloligands • photochemistry • platinum complexes • vapochromism

Introduction

The reaction of PPh₂Cl with primary amines in the presence of NEt₃ represents a simple and efficient synthetic method for the preparation of α -aminophosphines.^[1] The commercial availability of a large number of functionalized amines facilitates the fine tuning of the stereoelectronic properties of this class of ligands. A systematic study of their coordination properties then becomes easier, as well as those of the catalytic and physical properties of their metal complexes.^[2] We recently reported the synthesis of the new ligand diphenylphosphino-2-amino-2-thiazoline (**1**), the formation

of which follows a non-trivial reaction pathway involving the intermediacy of the diphosphine Ph₂PN=CN-(PPh₂)CH₂CH₂S and phosphoryl migrations, as summarized in Scheme 1.^[3]

Ligand **1** readily leads to a stable bischelated platinum(II) complex featuring its deprotonated form, *cis*-[Pt(**1**_{-H})₂] (Scheme 1). Access to this complex can result from ligand deprotonation prior to chelation (Scheme 1), or from deprotonation of a dicationic bischelated complex, by taking advantage of the enhanced acidity of the NH moiety upon



Scheme 1.

[a] Dr. R. Pattacini, Dr. P. Braunstein
Laboratoire de Chimie de Coordination, Institut de Chimie
(UMR 7177 CNRS), Université Louis Pasteur, 4 rue Blaise Pascal
F-67070 Strasbourg Cedex (France)
Fax: (+33) 390-241-322
E-mail: braunstein@chimie.u-strasbg.fr

[b] C. Giansante, Prof. P. Ceroni, Prof. M. Maestri
Dipartimento di Chimica "G. Ciamician", Università di Bologna
via Selmi 2, I-40126 Bologna (Italy)
Fax: (+39) 051-2099-456
E-mail: paola.ceroni@unibo.it

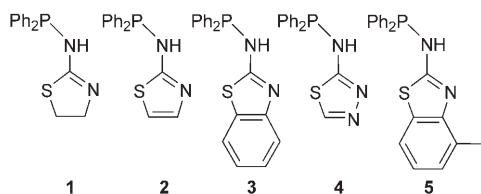
Supporting information for this article is available on the WWW
under <http://www.chemeurj.org/> or from the author.

P-coordination, which allows the use of bases weaker than *n*BuLi, such as NEt₃. Despite its remarkable stability, *cis*-[Pt(**1**-H)₂] easily reacts with electrophilic metal centers, giving rise, for instance, to the formation of the heterodimetallic Pt/Ag coordination polymer [Ag{Pt(**1**-H)₂}]_∞(OTf)_∞ (Scheme 1, OTf = CF₃SO₃⁻).^[3]

We wished to investigate the coordination properties of phosphino-thiazole and -thiazoline ligands, to study and compare their solution behavior and the reactivity of their transition metal complexes. Herein we report a comparative study on a series of bischelated platinum(II) complexes, which revealed that minor structural differences may result in remarkably different chemical and photophysical properties.

Results and Discussion

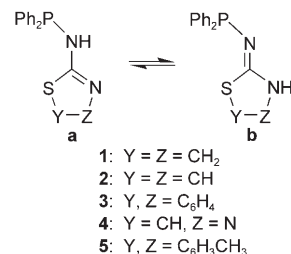
Synthesis of the Ligands: Diphenylphosphino-aminothiazoline (**1**),^[3] diphenylphosphino-aminothiazole (**2**),^[4] and diphenylphosphino-aminobenzothiazole (**3**)^[5] were prepared according to the literature procedures, by reaction of PPh₂Cl with the parent amine in the presence of NEt₃. An analogous approach was followed for diphenylphosphino-thiadiazole (**4**). Attempts to synthesize the diphenylphosphino-methyl-aminobenzothiazole (**5**) following the strategy used for **1–4** were unsuccessful, as Ph₂P(O)PPh₂ was formed in ≈30% yield. This is due to the fact that amino-4-methylbenzothiazole competes with NEt₃ as HCl scavenger, leaving a significant amount of PPh₂Cl unreacted, which in turn is hydrolyzed to Ph₂P(O)PPh₂. This would imply that amino-4-methylbenzothiazole has a higher basicity than aminobenzothiazole. This may stem from the steric hindrance induced by the methyl group, which prevents the formation of pseudodimers of the type of those reported in Scheme 3 (see below). Consequently, ligand **5** was prepared by reaction of the parent amine with PPh₂Cl in a 2:1 ratio, without the use of an external base.



Despite the simplicity of the preparation procedure, a study of the reaction mechanism leading to **1** revealed the involvement of an alternative pathway.^[3] Phosphine **1** is in fact the thermodynamic product of a multi-step reaction, the diphosphine Ph₂PN=C(N(PPh₂))CH₂CH₂S is initially formed by the attack of PPh₂Cl first on the endo-cyclic nitrogen of the amine, and then on the exo-cyclic one (Scheme 1). Reaction of this diphosphine with the residual amine, followed by phosphoryl group migration, finally leads to the formation of **1**. This pathway was not observed

for ligands **2–5**, suggesting that in these cases the more nucleophilic exo-cyclic nitrogen is attacked first, yielding directly the desired monophosphine ligand.

Two tautomers of phosphines **1–5** are potentially present in solution, as depicted in Scheme 2.



Scheme 2.

Only the tautomeric form **a** has been reported in the literature for **2**^[6] and **3**,^[5] either in the solid state or in solution. The concentration-dependent chemical shift of 47–51 ppm for **1** suggested the presence in solution of both tautomers, in rapid equilibrium and in a ≈1:1 molar ratio.^[3] A convenient NMR reference for imino tautomers **b** is provided by the diphosphine Ph₂PN=C(N(PPh₂))CH₂CH₂S, whose exocyclic, iminophosphine-type ³¹P nucleus resonates at 52 ppm, in contrast to 42 ppm for the aminophosphine-type ³¹P nucleus.^[3] The ³¹P chemical shift of **2**, **3**, and **5** is in the range 42.5–44.5 ppm, values which are typical for aminophosphines (i.e., 43 ppm for bis(diphenylphosphino)amine, Ph₂PNHPPPh₂). The NMR spectroscopy data for **3** were recorded in CDCl₃ since, in contrast to a previous report,^[5] this phosphine is well soluble in chlorinated solvents and shows a moderate solubility in toluene. The different behavior of **1** compared to **2**, **3**, and **5** can be qualitatively explained by the ring heteroaromaticity of the latter, which decreases the basicity of the endo-cyclic nitrogen and thus, stabilizes tautomer **a**. The ³¹P chemical shift of **4** at 51.7 ppm indicates that tautomer **b** is the major species in solution, rather surprisingly in view of the low basicity of the thiadiazole ring.

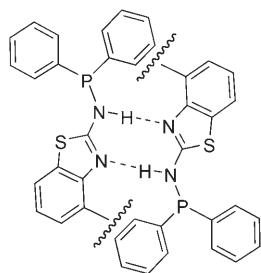
Ligands **1** and **4** rapidly undergo alcoholysis and react with CH₃OH to form the respective phosphinite and the parent aminothiazoline. Since **2**, **3**, and **5** degrade more slowly, the kinetics of this reaction appear to depend on the availability in solution of tautomer **b**. The tautomers observed in solution and the reactivity of **1–5** towards alcoholysis are summarized in Table 1, together with the observed ³¹P NMR chemical shifts.

In comparison with **1–4**, phosphine **5** is much more soluble in organic solvents. The methyl group probably hinders the formation of the pseudo-dimers typically observed in the solid state (see for example, Scheme 3). Consistently the NH NMR signal of **5** was not detected, even in concentrated solutions of **5** in CDCl₃, in contrast to those of **1–4**, which are in more rigid environments.

Table 1. Tautomers observed in solution for phosphines **1–5** and reactivity towards alcoholysis.

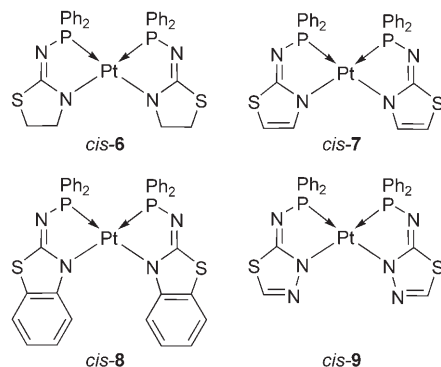
Ligand	Tautomer observed	³¹ P NMR δ [ppm]	Reactivity towards alcoholysis [h] ^[a]
1	a/b	47–52	≈2
2	a	42.3	≈48
3	a	44.5	≈40
4	b	51.7	≈2
5	a	43.0	≈48

[a] 10:1 excess of MeOH in CDCl₃, 100% conversion time.



Scheme 3.

Bischelated platinum(II) complexes: Two equivalents of aminophosphines **1–4** were reacted with [PtCl₂(NCPh)₂] in the presence of NEt₃ to form the complexes *cis*-[Pt(**1**-H)₂] (*cis*-**6**), *cis*-[Pt(**2**-H)₂] (*cis*-**7**), *cis*-[Pt(**3**-H)₂] (*cis*-**8**) and *cis*-[Pt(**4**-H)₂] (*cis*-**9**), respectively, in almost quantitative yields.



The poor solubility of these neutral, bischelated complexes in MeCN facilitates their purification. Their X-ray molecular structures are depicted in Figures 1–4 and selected bond distances and angles are compared in Table 2. In these complexes, two deprotonated ligands **1–4**, respectively, chelate the metal centre through the phosphorous and the endo-cyclic nitrogen atoms. Although they display similar geometrical parameters (Table 2), some structural details deserve comments.

In complex *cis*-**6**, the C=N double bond is more delocalized over the N–C–N unit than in *cis*-**7–9**, the distances are similar (C1–N1 1.321(5) and C2–N2 1.327(5) Å; C16–N3 1.332(5) and C16–N4 1.317(5) Å). In contrast, the exo-cyclic C1–N1 bond in *cis*-**7–9** has more double bond character than the endo-cyclic C1–N2 bond. The average S–C3 and N2–C2 distances are longer in *cis*-**6** than in the other three complexes, as a result of the non-aromaticity of the thiazole ring. The value of the latter influences the bond order C1–N2. Two resonance forms can be formally envisaged for complexes *cis*-**6–9**, see an example (*cis*-**6**) in Scheme 4.

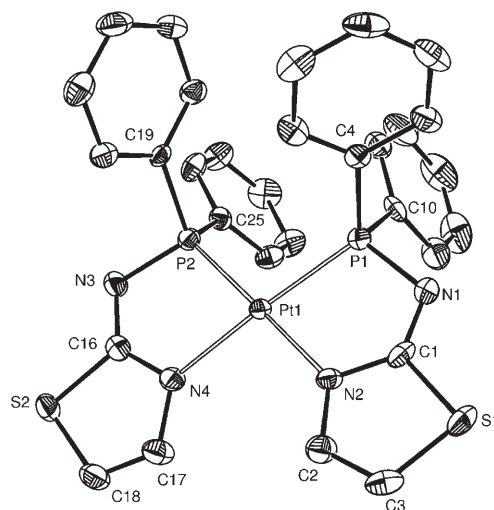


Figure 1. View of the molecular structure of compound *cis*-**6**·2CH₃OH·CH₃CN (Displacement parameters include 50% of the electron density).

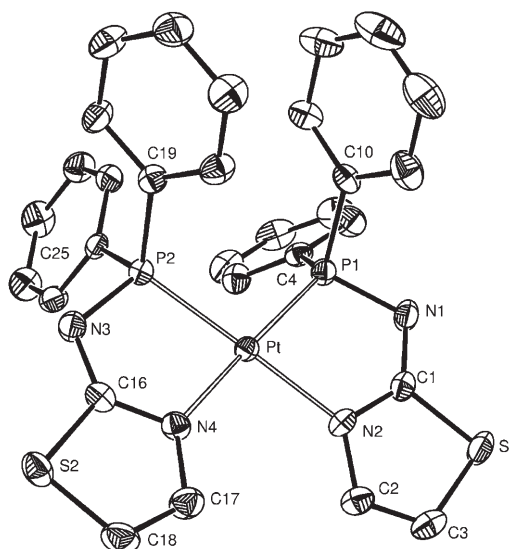
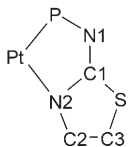


Figure 2. View of the molecular structure of compound *cis*-**7** (Displacement parameters include 50% of the electron density).

While for *cis*-**7–9** form **b** is more appropriate, on the basis of structural parameters, resonance form **a** contributes significantly to the bonding in *cis*-**6**, which should result in a more nucleophilic character for the two exocyclic nitrogen atoms and consequently, in their enhanced reactivity toward electrophilic metal centers. We shall see below that this is confirmed by the experimental observations.

Complex *cis*-**6** co-crystallized with two molecules of CH₃OH and one of CH₃CN. The CH₃OH molecules form hydrogen bonds with the exo-cyclic nitrogen atoms of the complex to form CH₃OH···*cis*-**6**···HOCH₃ entities (O1···N1 and O2···N3 separations: 2.813(5) and 2.809(5) Å, respectively) as illustrated in Figure 5.

Table 2. Selected bond distances [\AA] for compounds *cis-6-9*, together with a common atoms numbering scheme.



	<i>cis-6</i>	<i>cis-7</i>	<i>cis-8</i>	<i>cis-9</i>
av. P–Pt	2.238(1)	2.2482(8)	2.245(2)	2.2525(8)
av. N–Pt	2.095(3)	2.106(2)	2.121(4)	2.071(3)
av. N–P	1.663(3)	1.663(3)	1.673(5)	1.668(2)
av. C1–N1	1.326(5)	1.315(4)	1.316(7)	1.316(3)
av. C1–N2	1.322(5)	1.355(4)	1.357(7)	1.356(3)
C1–S	1.765(4)	1.751(3)	1.752(6)	1.746(6)
C3–S	1.799(4)	1.728(3)	1.745(7)	1.742(7) (C1–S2)
N2–C2	1.472(4)	1.382(4)	1.410(7)	1.381(8) (N2–N3)

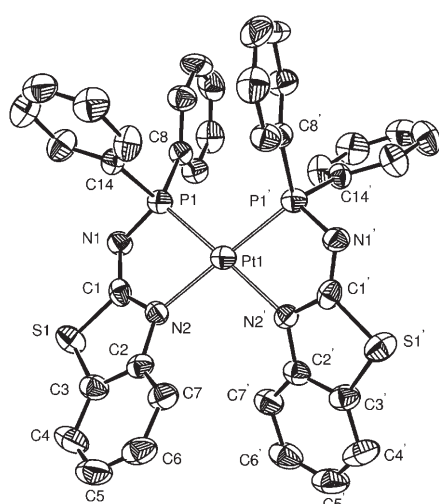


Figure 3. View of the molecular structure of compound *cis-8* in *cis-8*·2CHCl₃ (Displacement parameters include 50% of the electron density). Symmetry operations generating equivalent atoms ('): $-x, -y, z$.

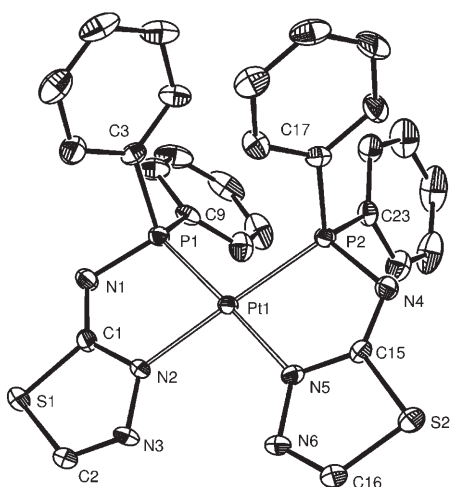
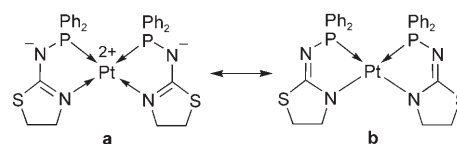


Figure 4. View of the molecular structure of compound *cis-9* (Displacement parameters include 50% of the electron density).



Scheme 4.

The acetonitrile methyl groups connect the $\text{CH}_3\text{OH}\cdots\text{cis-6}\cdots\text{HOCH}_3$ moieties through $\text{H}\cdots\text{O}$ contacts, in such a way that infinite chains of formula *cis-6*·2CH₃OH·CH₃CN are formed. These chains are furthermore interconnected by $\text{H}\cdots\text{Pt}$ contacts between **6** and the remaining methyl hydrogen of CH₃CN ($\text{C}_{\text{CH}_3}\cdots\text{Pt1}$ separation: 3.905(3) \AA). The intra-chain and inter-chain Pt \cdots Pt separations are 9.8673(2) and 16.0880(3) \AA , respectively.

As far as the metal–ligand bond lengths are concerned, we note that the Pt–N bond distances increase in the sequence *cis-9* < *cis-6* < *cis-7* < *cis-8*, probably as the result of the increasing mutual repulsion of the groups in α -position to the coordinating nitrogen. This effect is maximized for complex *cis-8*, in which the benzyl groups condensed to the thiazole ring induce a helicoidal distortion around the metal (Figure 6), as exemplified by the P1, P1', N1', N1 torsion angle of 9.5(4) $^\circ$.

In contrast to the situation in complexes *cis-6-9*, the Pt–P1–N1–C1–N2 ring of *cis-8* is not planar and adopts an envelope conformation, the angle formed by the planes passing through Pt1, P1, N1 and N1, C1, N2 being 24.7(5) $^\circ$.

The $^{31}\text{P}\{^1\text{H}\}$ NMR spectra chemical shifts for *cis-6-8* are at ≈ 65 ppm with $^1J(^{31}\text{P},^{195}\text{Pt})$ coupling constants ≈ 3350 Hz, while a slight downfield shift is observed for *cis-9*, with a resonance at 69.6 ppm.

Although all these complexes were synthesized in almost quantitative yields, an additional peak at 83.0 ppm in the ^{31}P NMR spectrum of *cis-9* was detected, in a $\approx 1:50$ integration ratio with respect to the main peak, with ^{195}Pt satellites displaying a $^1J(^{31}\text{P},^{195}\text{Pt})$ coupling constant of 2623 Hz. An analysis of the crystal morphologies revealed the presence of two distinct types of crystals. An X-ray diffraction analysis of the less abundant one allowed its identification as *trans*-Pt(**4**_{-H}) (*trans-9*). An ORTEP view of its molecular structure is shown in Figure 7.

In this centrosymmetric molecule, two deprotonated ligands **4** chelate the metal center in a *trans* arrangement of the donor atoms. As a result of the mutual trans influence of the phosphorus donors, the average P–Pt distance is longer in *trans-9* (2.313(2) \AA) than in *cis-9* (2.252(1) \AA), while the N–Pt bonds are shorter (2.011(5) \AA for *trans-9* vs. 2.071(3) \AA for *cis-9*). The chelation angle remains almost unchanged. The ligand displays bond distances and angles similar to those observed in *cis-9*.

In the crystals of *trans-9*, the molecules are interconnected by double $\text{H}\cdots\text{N}$ contacts (intermolecular C2 \cdots N3 distance: 3.39(1) \AA), to form infinite chains that have Pt \cdots Pt separations of 9.3273(3) \AA (Figure 8).

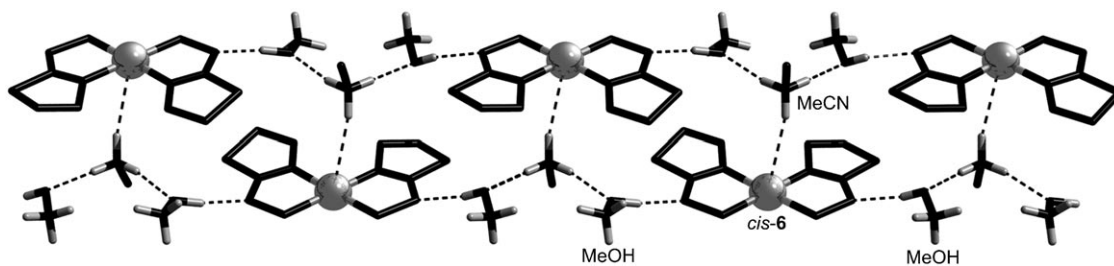


Figure 5. View of the crystal structure of *cis-6*-2CH₃OH-CH₃CN. Phenyl groups omitted for clarity. Symmetry operation generating equivalent molecules: $-x, -y, -z$; $-x, 1/2 + y, 1/2 - z$.



Figure 6. Views of the molecular structure of complex *cis-8* (phenyl groups omitted for clarity). Pt: gray spheres.

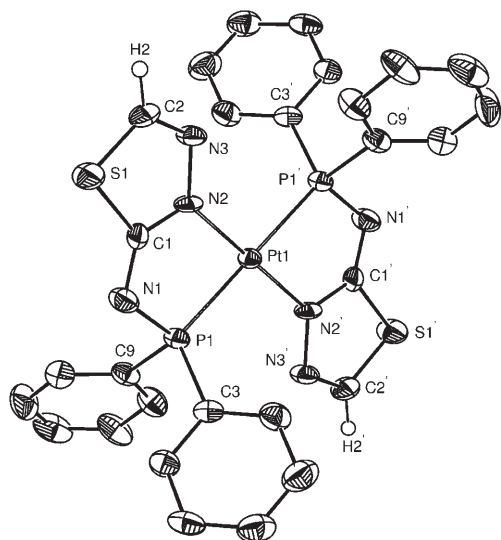


Figure 7. View of the molecular structure of compound *trans-9* (displacement parameters include 50% of the electron density). Selected bond distances [Å] and angles [°]: N2–Pt1 2.011(5), P1–Pt1 2.3133(18), N1–P1 1.668(6), C1–N1 1.304(8), C1–N2 1.360(9), C2–N3 1.288(9), C1–S1 1.756(6), C2–S1 1.721(8), N2–Pt1–P1 79.35(16), N2–Pt1–P1 100.65(16). Symmetry operation generating equivalent atoms ('): $-x, -y, -z$.

The Pt^{II} *trans* isomer has only been detected for ligand **4**, which is surprising, as the steric repulsion between the substituents in a position to the coordinated nitrogen atoms is minimized in the *trans* vs. the *cis* isomer. Although *cis-8* features a pronounced repulsion between the benzo groups condensed to the thiazole ring (see above), no trace of the *trans* isomer could be detected. The steric repulsion between the phenyl groups and the thiazole ring is minimized in *trans-9* as compared to the hypothetical *trans*-isomers of *cis-6-8*. Moreover, multiple intramolecular contacts between

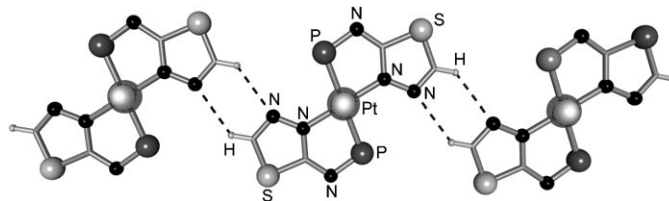


Figure 8. View, along the c^* axis of the crystal packing of compound *trans-9*. Symmetry operation generating equivalent molecules: $1 + x, y, z$, and $1 - x, y, z$.

the non-coordinated thiadiazole nitrogen atom and the phenyl protons may contribute to the stabilization the *trans* arrangement.

Reactivity of the Pt^{II} metalloligands towards Au^I complexes:

As indicated above, the C1–N2 bond of *cis-6* is shorter than in *cis-7-9* and *trans-9*, which results in a larger contribution of form **a** to the bonding (Scheme 4) and results in a higher nucleophilicity of the nitrogen atom in the α position to phosphorus. Reactions with electrophilic metal centers are indeed faster with *cis-6* than with complexes *cis-7-9* and *trans-9*.

Complexes *cis-6-9* were reacted with [AuCl(tht)] (tht = tetrahydrothiophene) in 1:1 and 1:2 ratios. Although coordination of AuCl fragments was observed for all the metalloligands, the reactions with *cis-7-9* resulted in unstable compounds which quickly decomposed with the formation of gold mirrors. Only in the case of *cis-6* we were able to isolate stable compounds, namely [*cis-6*(AuCl)] (**10**) and [*cis-6*(AuCl)₂] (**11**). ORTEP views of **10** in 10·3CHCl₃ and **11** in 11·2CH₂Cl₂ are shown in Figure 9 and Figure 10, respectively. Selected bond distances and angles are reported in Table 3.

Both **10** and **11** are neutral dimetallic complexes. In **10** only one of the exo-cyclic nitrogen atoms of *cis-6* is coordinated to an AuCl group whereas in **11**, each exo-cyclic N atom is coordinated to an AuCl group as a 2e donor. Coordination of the neutral Au^I fragments to *cis-6* leaves the geometrical parameters of the latter almost unchanged, with only a small change on the N–C distances in the NCN groups. In **10**, the N1–C1 distance (1.346(7) Å) is only slightly longer than N3–C16 (1.322(7) Å) and than N1–C1

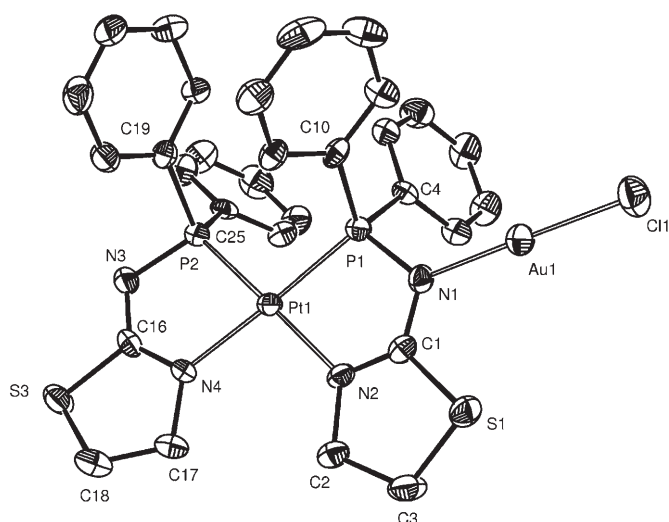


Figure 9. View of the molecular structure of compound **10** in **10**·3 CHCl₃ (Displacement parameters include 50% of the electron density).

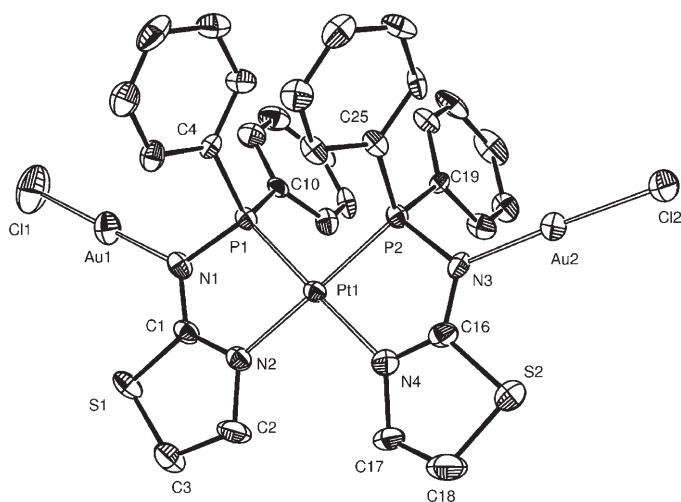


Figure 10. View of the molecular structure of compound **11** in **11**·2 CH₂Cl₂ (Displacement parameters include 50% of the electron density).

Table 3. List of selected bond distances [Å] and angles [°] for compounds **10** in **10**·3 CHCl₃ and **11** in **11**·2 CH₂Cl₂.

	10	11		10	11
Au1–Cl1	2.254(2)	2.242(3)	N2–C1	1.305(7)	1.324(11)
Au2–Cl2	–	2.249(2)	N3–C16	1.322(7)	1.346(10)
Au1–N1	2.032(4)	2.028(7)	N4–C16	1.335(7)	1.302(12)
Au2–N3	–	2.027(7)	Cl1–Au1–N1	179.2(2)	178.4(2)
P1–N1	1.676(5)	1.680(7)	Cl2–Au2–N3	–	178.0(2)
P2–N3	1.665(5)	1.689(7)	P1–Pt1–N2	80.6(2)	80.9(2)
P1–Pt1	2.235(2)	2.236(2)	P2–Pt1–N4	79.7(2)	81.3(2)
P2–Pt1	2.250(2)	2.233(2)	P1–N1–C1	114.2(4)	115.3(6)
N2–Pt1	2.094(4)	2.093(7)	P2–N3–C16	111.6(4)	113.5(6)
N4–Pt1	2.080(4)	2.115(7)	N1–C1–N2	124.2(5)	122.1(8)
N1–C1	1.346(7)	1.354(11)	N3–C16–N4	126.8(5)	126.2(8)

in *cis*-**6** (1.326(5) Å), while a shortening of the N2–C1 distance is observed (1.305(7) Å) compared to N4–C16

(1.335(7) Å) and to N2–C1 in *cis*-**6** (1.327(5) Å). A similar trend is observed for complex **11**.

The Pt/Au complexes **10** and **11** are stable and no degradation was observed upon exposure to air or moisture for days. Although **10** was obtained in good yields, traces of compound **11** were always observed, even if [AuCl(tht)] was used in default. This implies that the addition of a second equivalent of AuCl to *cis*-**6** is only slightly slower than the first. Compound **10** could be easily separated from **11** by fractional crystallization. We noticed that when cycles of dissolution in common solvents followed by evaporation of the solvent to dryness were applied to **10** and **11**, the quantity of complex dissolved gradually decreased, without appreciable decomposition. Compounds **10** and **11** slowly, and almost quantitatively, crystallize from their freshly prepared saturated CHCl₃ and CH₂Cl₂ solutions, respectively.

Although typical for terminal AuCl moieties, no close Au···Au contacts are present in the crystal structures of **10** and **11** (minimum Au···Au separations: 6.3842(4) for **10** and 6.824(2) Å for **11**). The chlorine atoms of **10** are in fact involved in multiple H···Cl contacts, in particular with the solvent and the thiazole protons (Figure 11). Pairs of molecules

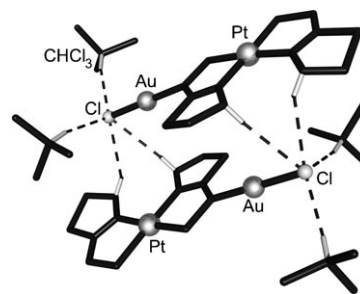


Figure 11. View of the crystal structure of **10**·3 CHCl₃, representing a pair of complexes, interconnected by H···Cl contacts and interacting with the solvent through the AuCl moiety. Dashed lines represent H···Cl contacts. White sticks represent the hydrogen atoms involved in these contacts. Protons and phenyls omitted for clarity.

adopt a head to tail arrangement and are disposed parallel to each other, forming layers of complex molecules, which are in turn separated by layers of solvent (Figure 12). Similar features are present in the crystal structure of **11**. In this case each CH₂Cl₂ molecule bridges two adjacent complexes and interacts with the AuCl groups through H···Cl contacts (Figure 13).

Examples of polynuclear compounds containing α -phosphino-amines and -imines bonded to two transition metal centers with both phosphorus and α -N have been reported in the literature. They include complexes featuring mutually interacting metal centers,^[7] dinuclear species bearing deprotonated Ph₂PNHPPPh₂ (dppa)^[8a-d] or Ph₂PNHC₆H₄NHPPPh₂,^[8c] phosphine functionalized macrocycles bridging transition metals^[9] and metal carbonyl clusters.^[10] At variance with their preparation, our strategy consisted of the reaction of an isolated, mononuclear, difunctional metalloligand, whose connectivity is fully maintained

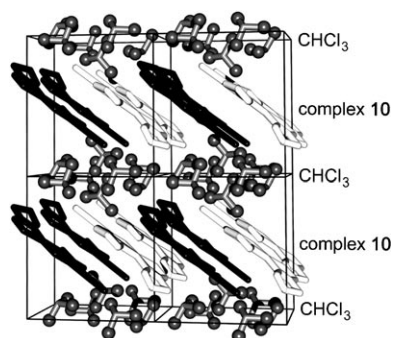


Figure 12. View of the crystal structure of **10**·3CHCl₃ along axis *c*, representing layers of parallel complex molecules separated by layers of solvent. Molecules of **10** oriented in the same direction are depicted with the same color.

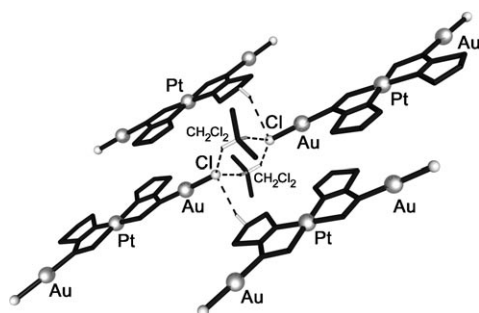


Figure 13. View of the crystal structure of **11**·2CH₂Cl₂. Dashed lines represent H...Cl contacts. White sticks represent the hydrogen atoms involved in these contacts. Protons and phenyls omitted for clarity.

in the heterodimetallic product. This procedure has been used previously,^[11] for example, with [Pd(dmba){Ph₂PN≡C(=O)Me}] (dmba = o-C₆H₄CH₂NMe₂) to afford the metal-metal bonded 1-D heterodimetallic coordination polymer [Ag{Pd(dmba)[Ph₂PN≡C(=O)Me]}]_∞.^[11b]

Photophysical properties of the Pt^{II} complex *cis-6*: Complex *cis-6* is the only one in the series that, upon exposure of the solid to CH₃OH vapors, displays a luminescence visible to the naked eye under excitation by using a conventional UV lamp (Figure 14). Moreover, crystals of *cis-6*·2CH₃OH·CH₃CN also displayed luminescence visible to the naked eye, unlike those of *cis-6*·C₆H₅CH₃.

This luminescent sensor property of *cis-6* prompted us to perform a detailed investigation of the photophysical properties of this complex, both in solution and in the solid state, in the presence or not of alcohol vapors, and as a function of temperature.

Photophysical properties of complex *cis-6* in solution: Complex *cis-6* absorbs only in the UV region of the spectrum with a maximum at 300 nm (Figure 15). At 298 K solutions of *cis-6* in alcohols (C₂H₅OH:CH₃OH, 4:1 v/v) 2-methyltetrahydrofuran, chlorinated solvents (CH₂Cl₂:CHCl₃, 1:1 v/v) or butyronitrile do not exhibit luminescence, either in air-



Figure 14. Photograph of an aluminum foil covered by a thin layer of the dry complex *cis-6* (≈ 5 mg on a 12×5 cm surface) exposed to the radiation of a common UV lamp for TLC analysis, at a wavelength of ≈ 385 nm. The emission is restricted to areas in which the layer was treated with drops of CH₃OH.

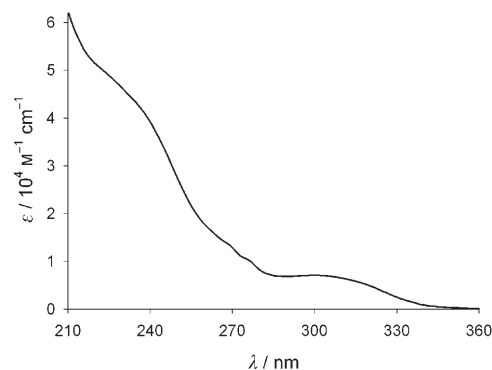


Figure 15. Absorption spectrum of complex *cis-6* in CH₃OH solution at 298 K.

equilibrated or in argon-saturated conditions, while in rigid matrix at 77 K a strong luminescence occurs (Figure 16). Slight changes in the band maximum, shape and excited-state lifetimes (Table 4) and more pronounced differences in the relative emission intensities were observed as a function of solvent.

The nature of the emitting excited state is not easy to ascertain. A simplified classification based on a localized molecular orbital approach^[12] (metal- or ligand-centered,

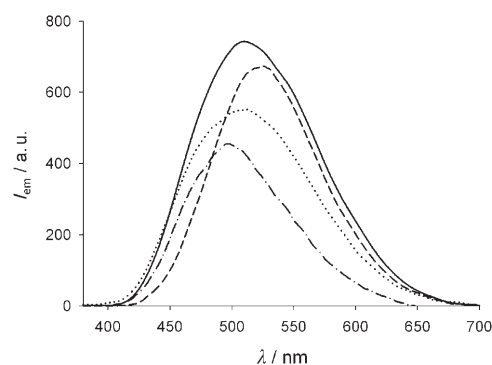


Figure 16. Emission spectra of complex *cis-6* in rigid matrix at 77 K of C₂H₅OH:CH₃OH, 4:1 v/v (solid line), CH₂Cl₂:CHCl₃, 1:1 v/v (dashed line), butyronitrile (dotted line), and 2-methyl tetrahydrofuran (dashed-dotted line). Emission intensities are directly comparable since these solutions have the same absorbance at the excitation wavelength ($\lambda_{\text{ex}} = 315$ nm).

Table 4. Photophysical properties of complex *cis-6* in rigid matrix at 77 K. Relative intensities are directly comparable since the investigated solutions have the same absorbance at the excitation wavelength ($\lambda_{\text{ex}} = 315$ nm).

Matrix	λ_{max} [nm]	I_{rel} [a.u.]	τ [μs]
C ₂ H ₅ OH:CH ₃ OH, 4:1 v/v	510	100	25
CH ₂ Cl ₂ :CHCl ₃ , 1:1 v/v	525	90	15
butyronitrile	510	75	20
2-methyl tetrahydrofuran	495	60	20

metal-to-ligand or ligand-to-metal charge transfer) is not satisfactory for this platinum(II) complex as states of mixed nature are likely to exist.^[13] The rather long lifetime and the large energy difference between absorption and emission bands suggest that this excited state is formally a triplet. Free ligand **1** in a butyronitrile rigid matrix shows an unstructured and very weak phosphorescence band with a maximum at 440 nm, insensitive to solvent polarity and with a longer lifetime ($\tau \approx 5$ ms) compared to complex *cis-6*. The phosphorescence band maximum of complex *cis-6* is red-shifted compared to that of free ligand **1** and is quite sensitive to solvent nature and temperature (vide infra), suggesting that the corresponding transition is not merely ligand centered, but has charge-transfer character.

As a result of the huge increase of luminescence intensity for complex *cis-6* upon lowering the temperature from 298 to 77 K, we investigated in more detail the luminescence intensity and excited-state lifetimes as a function of temperature. Figure 17 shows the changes in emission lifetime and band maximum for butyronitrile solution (similar results have been obtained in a CH₂Cl₂:CH₃OH mixture) from 85 to 125 K. A strong discontinuity is present in the temperature range 100–120 K, in which the band maximum shifts strongly to the red (from 495 to 550 nm), the luminescence intensity decreases by a factor of ≈ 20 and the excited-state lifetime slightly decreases (by about a third). At temperatures above 125 K, no substantial change in the emission band shape and position is observed in comparison to those

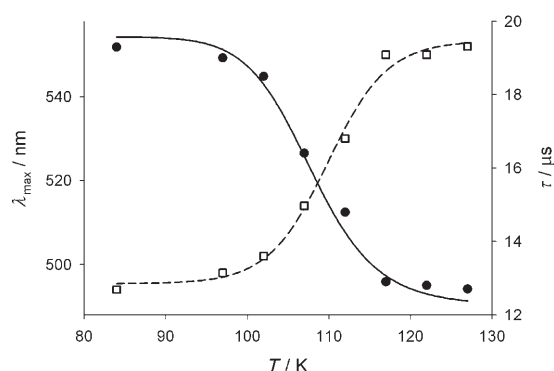


Figure 17. Emission lifetime (solid circles, right axis) and emission band maximum (empty squares, left axis) as a function of temperature for complex *cis-6* in butyronitrile. $\lambda_{\text{ex}} = 315$ nm. The solid line represents the fitted curve according to Equation (1).

recorded at 120 K, but the emission intensity decreases and complete loss of luminescence occurs above 160 K. In this temperature range, butyronitrile becomes completely fluid ($T_f = 161$ K) and deactivation by non-radiative processes becomes faster.

Red-shifts of the emission bands, upon increasing temperature, have been reported for other complexes in which the emitting excited state has a charge transfer character.^[14,15] This phenomenon is a rigidochromic effect;^[16] a large color change of an emission as a function of the rigidity (viscoelasticity) of the medium. Matrix softening may remove viscosity-dependent potential barriers presented by the solvent cage, thus, enabling the complex to relax to lower energy nuclear configurations corresponding to smaller equilibrium distances between the metal centre and the ligands, not accessible in a rigid matrix.^[15] According to this model, decrease of lifetimes (τ) can be accounted for by an additional radiationless decay process of the emitting excited state as the temperature increases. In particular, values of τ can be fitted (solid line in Figure 17) according to the following empirical formula [Eq. (1)]:^[14]

$$\frac{1}{\tau} = \frac{k_0 + B}{\{1 + \exp[C(1/T - 1/T_B)]\}} \quad (1)$$

This describes a stepwise behavior centered at temperature T_B (k_0 is a temperature-independent term, B is the value attained by $1/\tau$ at $T \gg T_B$ and C is a temperature related to the smoothness of the step). At low temperatures (85–100 K in the present case), vibrational motions of the complex occur much faster than reorientational and translational rearrangements of the solvent molecules, so that the solvent medium behaves as a rigid cage and some radiationless processes, in particular the low-frequency ones, are inhibited. The fitting of the data with this model in the temperature range 85–125 K is good and leads to a value of $T_B = 110$ K.

Photophysics of complex *cis-6* in the solid state: To better understand the aforementioned effect of CH₃OH on the luminescence of complex *cis-6*, we have investigated the emission properties of a solid sample obtained by evaporation from toluene solution before and after exposure to CH₃OH vapors at room temperature. In the presence of CH₃OH a much stronger luminescence^[17] is observed (Figure 18) with a maximum shifted to the blue (Table 5).

This vapoluminescence effect observed upon exposure to CH₃OH vapors of complex *cis-6* crystallized from toluene, cannot be attributed to a disruption of intermolecular Pt...Pt interactions, as in the case of previously reported Pt^{II} complexes.^[18] Indeed, the single crystal X-ray diffraction analysis of complex *cis-6* crystallized from toluene, *cis-6*·C₆H₅CH₃, revealed a molecular structure almost identical to that found in *cis-6*·2 CH₃OH·CH₃CN, with a shorter minimum Pt...Pt intermolecular distance: 5.9267(2) Å for *cis-6*·C₆H₅CH₃ and 8.9268(2) Å for *cis-6*·2 CH₃OH·CH₃CN. The crystal data for *cis-6*·C₆H₅CH₃ are reported in the CIF file deposited in the CCDC database (CCDC code: 653227). In

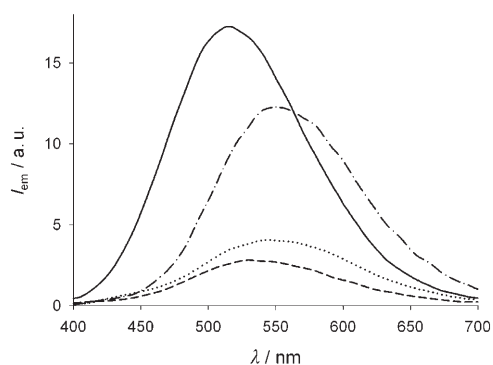


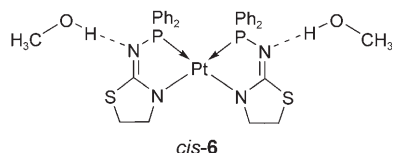
Figure 18. Emission spectra of complex *cis-6* crystallized from toluene (dashed line) or exposed to CH_3OH (solid line), $\text{CH}_3\text{CH}_2\text{OH}$ (dashed-dotted line), or $(\text{CH}_3)_2\text{CHOH}$ (dotted line) at room temperature. $\lambda_{\text{ex}} = 313 \text{ nm}$.^[17]

Table 5. Photophysical properties of complex *cis-6* at 298 and 77 K for solid samples exposed to different alcohol vapors. $\lambda_{\text{ex}} = 315 \text{ nm}$.

Vapor	298 K		77 K	
	λ_{max} [nm]	τ [μs]	λ_{max} [nm]	τ [μs]
[a]	530	0.2, 1.0	520	20
CH_3OH	520	0.2, 1.0	505	20
$\text{CH}_3\text{CH}_2\text{OH}$	550	0.2, 1.0	540	20
$(\text{CH}_3)_2\text{CHOH}$	540	0.2, 1.0	530	20

[a] Crystals obtained by toluene solutions without exposure to any alcohol vapor.

the solid state structure of *cis-6*·2 CH_3OH · CH_3CN , a CH_3OH molecule forms a hydrogen bond with each exo-cyclic nitrogen atoms of the complex (Figure 5 and Scheme 5).



Scheme 5.

Because of the *structural* effect of the $\text{N}\cdots\text{HOCH}_3$ hydrogen bonding, complex *cis-6*·2 CH_3OH · CH_3CN has a more rigid structure than *cis-6*· $\text{C}_6\text{H}_5\text{CH}_3$. This may explain the increase of emission quantum yield, because deactivation by non-radiative decays is slower in a more rigid structure. Remarkable electronic effects of this hydrogen bonding on *cis-6* and therefore on the luminescence properties are unlikely. The NMR spectroscopic data of *cis-6* in CH_3OH solutions are in fact very similar to those in CDCl_3 and the molecular structures of *cis-6* in *cis-6*·2 CH_3OH · CH_3CN and in *cis-6*· $\text{C}_6\text{H}_5\text{CH}_3$ are almost identical. In the crystals of *cis-6*·2 CH_3OH · CH_3CN molecules of acetonitrile were also present. On the other hand, acetonitrile vapors did not lead to luminescent properties for dry *cis-6*.

A vapoluminescent effect was also observed upon exposure of solid *cis-6* to $\text{CH}_3\text{CH}_2\text{OH}$ (Figure 18), but the increase in the luminescence intensity is lower and the band maximum is more shifted to the red (Table 5). $(\text{CH}_3)_2\text{CHOH}$ has a very modest effect (Figure 18), a slight increase in emission intensity and small red-shift of the band maximum (Table 5), whereas $\text{CH}_3(\text{CH}_2)_3\text{OH}$ does not lead to any significant increase in luminescence or change in the emission band maximum. Luminescence intensity decays of these solid samples are multiexponential and they can be fitted by using two families of lifetimes ($\tau_1 \approx 0.2 \mu\text{s}$, $\tau_2 \approx 1.0 \mu\text{s}$) in which the percentage of the longer lifetime increases upon increasing emission quantum yield.

The solid samples discussed above show a much stronger luminescence at 77 K, a lifetime of 20 μs , and a significantly blue-shifted emission maximum compared to the corresponding values at room temperature (Table 5), confirming the charge transfer character of the corresponding electronic transition. The emission bands recorded under these experimental conditions are very similar in shape and position to those recorded in the corresponding rigid matrix. Therefore, the emission in the solid state is of the same nature as that observed for diluted solutions ($\approx 5 \times 10^{-5} \text{ M}$) at 77 K, and is a property of the isolated molecule, thus confirming that Pt··Pt interactions do not play any role in the luminescence properties of these solid samples.

Conclusion

By analogy with complexes containing a coordinated P,O-phosphanyl enolate ligand,^[2a] which react with softer electrophiles such as transition metal centers at the enolate carbon α to P, we have provided here further examples showing that complexes containing an isoelectronic P,N-phosphanyl iminolate chelate can also lead to heterodimetallic complexes in a controlled way. With the latter systems, the advantage is that the coordination geometry of the P–N nitrogen atom remains planar upon metalation, which simplifies the stereochemical issues one encounters with the corresponding P–C system since upon metalation, the carbon atom becomes a sp^3 -hybridized stereogenic center.^[21]

We have found that rather minor stereoelectronic differences in the ligands may significantly affect the chemical and physical properties of the related complexes. The vapoluminescence properties of *cis-6* prompts us to study the coordination properties of ligand **1** toward less precious metals, to fine tune their potential activity as sensors. The rationalization of the unprecedented H-bonding rigidochromic effect of the alcohol will allow us to better tune these structural and physical properties.

Experimental Section

General Considerations: All manipulations were carried out under inert dinitrogen atmosphere, using standard Schlenk-line techniques and dried

and freshly distilled solvents. The ^1H , $^{13}\text{C}\{^1\text{H}\}$, and $^{31}\text{P}\{^1\text{H}\}$ NMR spectra were recorded at 298 K by using a Bruker Avance 300 instrument at 300.13, 75.47 and 121.49 MHz, respectively, using TMS or H_3PO_4 (85% in D_2O) as external standards with downfield shifts reported as positive. All NMR spectra were measured at 298 K. The assignment of the signals was made by ^1H , ^1H -COSY and ^1H , ^{13}C -HMBC experiments. Elemental C, H, and N analyses were performed by the "Service de microanalyses", Université Louis Pasteur, Strasbourg. The following compounds were prepared according to literature procedures: $[\text{PtCl}_2(\text{NCPH}_2)]$,^[19] $[\text{AuCl}(\text{tht})]$,^[20] **1**,^[3] and **2**.^[4] PPh_2Cl and NEt_3 were freshly distilled before use. Other chemicals were commercially available and used as received.

Preparation of ligand 3: Ligand **3** was prepared using a method similar to that already reported.^[5] In contrast to the literature data, a high solubility in chlorinated solvents was observed. The NMR data recorded in CDCl_3 are listed below. ^1H NMR (CDCl_3 , the labeling of the atoms refers to that of the ligand in the ORTEP plot of *cis-8* (Figure 3): $\delta=6.85$ (m, 1H; H7), 7.25–7.40 (m, 6H; *m,p*-Ph), 7.07 (m, 2H; H5, H6), 7.43 (m, 4H; *o*-Ph), 7.59 (m, 1H; H4), 8.81 ppm (s br, 1H; NH); $^{13}\text{C}\{^1\text{H}\}$ NMR (CDCl_3): $\delta=119.2$ (s; C7), 120.9 (s; C4), 122.3 (s; C5), 125.8 (s; C6), 128.7 (d, $^3J(\text{C,P})=6.9$ Hz; *m*-Ph), 129.7 (s, *p*-Ph), 131.3 (d, $^1J(\text{C,P})=13.8$ Hz; C3), 131.4 (d, $^2J(\text{C,P})=20.5$ Hz; *o*-Ph), 137.5 (d, $^1J(\text{C,P})=8.2$ Hz; *i*-Ph), 151.1 (s; C2), 171.2 ppm (d, $^2J(\text{C,P})=34.8$ Hz; C1); $^{31}\text{P}\{^1\text{H}\}$ NMR (CDCl_3 , saturated solution) $\delta=44.5$ ppm (s); elemental analysis calcd (%) for $\text{C}_{19}\text{H}_{15}\text{N}_2\text{PS}$ (334.38): C 68.25, H 4.52, N 8.38; found: C 68.37, H 4.74, N 8.61.

Preparation of ligand 4: Liquid Ph_2PCL (1.82 mL, 9.9 mmol) was added dropwise to a solution of amino-thiadiazole (2.00 g, 19.8 mmol) in THF (100 mL). The solution was stirred for 6 h, amino-thiadiazolium chloride was removed by filtration, the volatiles were removed under reduced pressure and the colorless solid obtained was dissolved in a minimum amount of THF. Pentane was slowly layered onto the THF solution yielding **4** as colorless crystals, which were then washed with Et_2O (2×50 mL). Yield: 2.35 g, 83%. ^1H NMR (CDCl_3): $\delta=7.33$ –7.43 (m, 6H; *m,p*-Ph), 7.46–7.57 (m, 4H; *o*-Ph), 8.43 ppm (d, $^3J(\text{H,P})=2.3$ Hz, 1H; N=CH); $^{13}\text{C}\{^1\text{H}\}$ NMR (CDCl_3): $\delta=128.8$ (d, $^3J(\text{C,P})=7.3$ Hz; *m*-Ph), 130.0 (s; *p*-Ph), 131.4 (d, $^2J(\text{C,P})=21.0$ Hz; *o*-Ph), 137.6 (d, $^1J(\text{C,P})=8.2$ Hz; *i*-Ph), 143.9 (d, $^4J(\text{C,P})=6.4$ Hz; N=CH), 172.4 ppm (d, $^2J(\text{C,P})=28.3$ Hz; N=C=N); $^{31}\text{P}\{^1\text{H}\}$ NMR (CDCl_3): $\delta=51.7$ ppm (s); elemental analysis calcd (%) for $\text{C}_{14}\text{N}_3\text{H}_{12}\text{PS}$ (285.30): C 58.94, H 4.24, N 14.73; found: C 59.18, H 4.15, N 14.39.

Preparation of ligand 5: Liquid Ph_2PCL (1.121 mL, 6.1 mmol) was added dropwise to a solution of 2-amino-4-methyl-benzothiazole (2.00 g, 12.2 mmol) in THF (100 mL). After the solution was stirred for 6 h, 2-amino-4-methyl-benzothiazolium hydrochloride was removed by filtration. Evaporation of the volatiles yielded compound **5** as a colorless powder. Yield: 1.91 g, 90%. ^1H NMR (CDCl_3 , The labeling of the atoms refers to that of ligand **3**): $\delta=2.51$ (m, 3H; CH_3), 7.02–7.13 (m, 2H; H5, H6), 7.30–7.60 ppm (m, 11H; Ph, H4); $^{13}\text{C}\{^1\text{H}\}$ NMR (CDCl_3): $\delta=18.4$ (s; CH_3), 118.6 (s; C4), 122.5 (s; C5), 126.9 (s; C6), 128.8 (d, $^3J(\text{C,P})=7.0$ Hz; *m*-Ph), 129.2 (s; C7), 129.9 (s; *p*-Ph), 131.4 (d, $^2J(\text{C,P})=20.7$ Hz; *o*-Ph), 131.6 (d, $^2J(\text{C,P})=12.2$ Hz; C3), 137.6 (d, $^1J(\text{C,P})=8.5$ Hz; *i*-Ph), 150.5 (s; C2), 168.8 ppm (d, $^2J(\text{C,P})=33.0$ Hz; N=C=N); $^{31}\text{P}\{^1\text{H}\}$ NMR (CDCl_3): $\delta=43.0$ ppm (s); elemental analysis calcd (%) for $\text{C}_{20}\text{H}_{17}\text{N}_2\text{PS}$ (348.4): C 68.95, H 4.92, N 8.04; found: C 68.92, H 5.00, N 7.94.

Preparation of complex cis-7: To a stirred solution of $[\text{PtCl}_2(\text{NCPH}_2)]$ (0.300 g, 0.63 mmol) in THF (100 mL), were added NEt_3 (0.500 mL, 3.59 mmol) and solid **2** (0.360 g, 1.27 mmol). Stirring was continued for 1 h and $\text{Et}_3\text{NH-Cl}$ was removed by filtration. The volatiles were removed under reduced pressure and the colorless powder obtained was washed with amounts of MeCN (5×10 mL). Evaporation of the volatiles gave pure compound **7** as a colorless powder. Yield: 0.446 g, 93%. ^1H NMR (CDCl_3 , for atom labeling, see ORTEP plot) $\delta=6.27$ (ddd, $^3J(\text{H,H})=4.5$ Hz, $^5J(\text{H,P})=2.7$ Hz, 1.9 Hz, 2H; SCH), 7.03–7.10 (m, 8H; *m*-Ph), 7.16 (dd, $^3J(\text{H,H})=4.5$ Hz, $^4+^5J(\text{H,P})=0.9$ Hz, 2H; NCH), 7.23–7.37 ppm (m, 12H; *o,p*-Ph); $^{13}\text{C}\{^1\text{H}\}$ NMR (CDCl_3): $\delta=104.3$ (s; C2, C17), 127.9–133.2 (m; Ph), 133.6 (s; C3, C18), 189.8 ppm (s; N=C=N); $^{31}\text{P}\{^1\text{H}\}$ NMR (CDCl_3) $\delta=66.0$ ppm (s, $^1J(\text{P,Pt})=3310$ Hz); elemental analysis

calcd (%) for $\text{C}_{30}\text{H}_{24}\text{N}_4\text{P}_2\text{PtS}_2$ (761.70): C 47.31, H 3.18, N 7.36; found: C 47.26, H 3.41, N 7.20.

Preparation of complexes cis-6, cis-8 and cis-9: The procedure described for complex *cis-7* was also applied to the synthesis of *cis-6*, *cis-8* and *cis-9*, by using 0.363, 0.423 and 0.362 g of phosphines **1**, **3** and **4**, respectively, instead of **2**. Yields: 0.463 g, 96% for *cis-6*; 0.483 g, 89% for *cis-8*; 0.361 g, 75% for *cis-9*.

Complex *cis-6* was recrystallized from a 2:2:1 $\text{CH}_2\text{Cl}_2/\text{CH}_3\text{OH}/\text{CH}_3\text{CN}$ solution, giving *cis-6-2CH}_3\text{OH}\cdot\text{CH}_3\text{CN}. Complexes *cis-8* and *cis-9* were recrystallized by layering pentane on their saturated CH_2Cl_2 solutions. The spectroscopic data for *cis-6* have been reported elsewhere.^[3]*

Spectroscopic data for cis-8: ^1H NMR (CDCl_3): $\delta=6.71$ (m, 2H; H6), 6.80–6.91 (m, 4H; H7, H5), 7.00–7.38 (m, 14H; *m,p*-Ph and H4), 7.53 ppm (m, 8H; *o*-Ph); $\text{C}\{^1\text{H}\}$ NMR (CDCl_3): $\delta=117.8$ (s; C7), 121.1 (s; C4), 121.2 (s; C5), 124.9 (s; C6), 128.1–133.2 (m; Ph), 129.9 (s, $^4J(\text{C,P})=13.8$ Hz; C3), 147.8 (s; C2), 187.2 ppm (s; N=C=N); $^{31}\text{P}\{^1\text{H}\}$ NMR (CDCl_3): $\delta=69.1$ ppm (s, with ^{195}Pt satellites, $^1J(\text{P,Pt})=3368$ Hz); elemental analysis calcd (%) for $\text{C}_{38}\text{H}_{28}\text{N}_4\text{P}_2\text{PtS}_2$ (861.81): C 52.96, H 3.27, N 6.50; found: C 52.87, H 3.24 N 6.73;

Spectroscopic data for cis-9: ^1H NMR (CDCl_3): $\delta=7.05$ –7.15 (m, 8H; *m*-Ph), 7.24–7.37 (m, 12H; *o,p*-Ph), 8.26 ppm (filled-in d with Pt satellites, simulated $^5J(\text{H,P})=4.0$ Hz, $^2J(\text{P,P})=12.2$ Hz, 2H; N=CH); $^{13}\text{C}\{^1\text{H}\}$ NMR (CDCl_3): $\delta=128.1$ –132.6 (m; Ph), 139.8 (m, $^4J(\text{C,P})=6.5$ Hz with $^2J(\text{P,P})=12.2$ Hz, value extracted from the phenyl carbon pattern m; N=CH), 188.4 ppm (s; N=C=N); $^{31}\text{P}\{^1\text{H}\}$ NMR (CDCl_3): $\delta=69.6$ ppm (s, with Pt satellites; $^1J(\text{P,Pt})=3326$ Hz); elemental analysis calcd (%) for $\text{C}_{28}\text{H}_{22}\text{N}_6\text{P}_2\text{PtS}_2$ (763.67): C 44.04, H 2.90, N 11.00; found: C 44.39, H 2.90, N 10.84.

Preparation of complex 10: A solution of $[\text{AuCl}(\text{tht})]$ (0.200 g, 0.62 mmol) in CH_2Cl_2 (10 mL) was added dropwise, over a period of 10 min, to a solution of *cis-6* (0.474 g, 0.62 mmol) in CH_2Cl_2 (50 mL). After the solution was stirred for 20 min, the volatiles were removed under vacuum. The colorless solid obtained was washed with Et_2O (3×20 mL) and then redissolved in a minimum amount of CH_2Cl_2 . After 2 days **10-2CH}_2\text{Cl}_2 crystallized. Yield: 0.402 g, 65%. ^1H NMR (CDCl_3): $\delta=3.58$ (m, $^3J(\text{H,H})\approx 7.2$ Hz, 4H; H3, H18), 4.52 (t, $^3J(\text{H,H})=7.12$ Hz, 2H; H17), 4.32 (t, $^3J(\text{H,H})=7.12$ Hz, 2H; H2), 7.0–7.50 ppm (m, 20H; Ph); $^{31}\text{P}\{^1\text{H}\}$ NMR (CDCl_3): $\delta=64.4$ (d, $^2J(\text{P,P})=11.7$ Hz, with ^{195}Pt satellites, $^1J(\text{P,Pt})=3152$ Hz; P2), 75.2 ppm (d, $^2J(\text{P,P})=11.7$ Hz, with ^{195}Pt satellites, $^1J(\text{P,Pt})=3300$ Hz; P1); the poor solubility of this complex prevented recording of good quality $^{31}\text{C}\{^1\text{H}\}$ NMR spectra; elemental analysis calcd (%) for $\text{C}_{30}\text{H}_{28}\text{N}_4\text{AuClP}_2\text{PtS}_2$ (997.0): C 36.09, H 2.83, N 5.61; found: C 35.91, H 2.77, N 5.63.**

Preparation of complex 11: A solution of $[\text{AuCl}(\text{tht})]$ (0.200 g, 0.62 mmol) in CH_2Cl_2 (10 mL) was added dropwise, over a period of 10 min, to a solution of *cis-6* (0.237 g, 0.31 mmol) in CH_2Cl_2 (30 mL). After the solution was stirred for 20 min, the volatiles were removed under vacuum. The colorless solid obtained was washed with Et_2O (3×20 mL) and then redissolved in a minimum amount of CHCl_3 . After 2 days **11-3CHCl}_3** crystallized. Yield: 0.331 g, 87%. $^{31}\text{P}\{^1\text{H}\}$ NMR (CDCl_3): $\delta=73.8$ ppm (s, with ^{195}Pt satellites, $^1J(\text{P,Pt})=3256$ Hz); ^1H NMR (CDCl_3): $\delta=3.58$ (t, $^3J(\text{H,H})=7.4$ Hz, 4H; SCH_2), 4.50 (t, $^3J(\text{H,H})=7.4$ Hz, 4H; NCH_2), 7.0–7.5 ppm (m, 20H; Ph); the poor solubility of this complex prevented recording of good quality $^{31}\text{C}\{^1\text{H}\}$ NMR spectra; elemental analysis calcd (%) for $\text{C}_{30}\text{H}_{28}\text{N}_4\text{Au}_2\text{Cl}_2\text{P}_2\text{PtS}_2$ (1230.6): C 29.28, H 2.29, N 4.55; found: C 28.78, H 2.22, N 4.36.

X-ray data collection, structure solution and refinement for compounds cis-6-2CH}_3\text{OH}\cdot\text{CH}_3\text{CN, cis-7, cis-8-2CHCl}_3, cis-9, trans-9, 10-3CHCl}_3, and 11-2CH}_2\text{Cl}_2: Suitable crystals for the X-ray analysis were obtained as described above. The intensity data was collected at 173(2) K on a Kappa CCD diffractometer^[22] (graphite monochromated MoK_α radiation, $\lambda=0.71073$ Å). Crystallographic and experimental details for the structures are summarized in Table 6. The structures were solved by direct methods (SHELXS-97) and refined by full-matrix least-squares procedures (based on F^2 , SHELXL-97)^[23] with anisotropic thermal parameters for all the non-hydrogen atoms. The hydrogen atoms were introduced into the geometrically calculated positions (SHELXS-97 procedures) and refined riding on the corresponding parent atoms. CCDC-653221 (*cis-*

Table 6. X-ray data collection and refinement parameters for compounds *cis*-6-2CH₃OH·CH₃CN, *cis*-7, *cis*-8-2CHCl₃, *cis*-9, *trans*-9, 10-3CHCl₃ and 11-2CH₂Cl₂.

	<i>cis</i> -6 ·2CH ₃ OH·CH ₃ CN	<i>cis</i> -7	<i>cis</i> -8 ·2CHCl ₃	<i>cis</i> -9	<i>trans</i> -9	10 ·3CHCl ₃	11 ·2CH ₂ Cl ₂
formula	C ₃₀ H ₂₈ N ₄ P ₂ PtS ₂ ·CH ₃ CN·2CH ₃ OH	C ₃₀ H ₂₄ N ₄ P ₂ PtS ₂	C ₃₈ H ₂₈ N ₄ P ₂ PtS ₂ ·2CHCl ₃	C ₂₈ H ₂₂ N ₆ P ₂ PtS ₂	C ₂₈ H ₂₂ N ₆ P ₂ PtS ₂	C ₃₀ H ₂₈ AuClN ₄ P ₂ PtS ₂ ·3CHCl ₃	C ₃₀ H ₂₈ Au ₂ Cl ₂ N ₄ P ₂ PtS ₂ ·2CH ₂ Cl ₂
<i>F</i> _w	870.85	761.68	1100.53	763.67	763.67	1356.23	1400.40
crystal system	monoclinic	monoclinic	monoclinic	triclinic	monoclinic	triclinic	triclinic
space group	<i>P</i> 2 ₁ / <i>c</i>	<i>P</i> 2 ₁ / <i>c</i>	<i>C</i> 2/ <i>c</i>	<i>P</i> $\bar{1}$	<i>P</i> 2 ₁ / <i>c</i>	<i>P</i> $\bar{1}$	<i>P</i> $\bar{1}$
<i>a</i> [Å]	12.5240(1)	14.8660(2)	24.7820(9)	11.3530(1)	9.3273(3)	11.7520(4)	9.175(5)
<i>b</i> [Å]	16.0880(2)	11.8280(2)	12.0870(4)	13.9230(2)	10.2960(6)	12.6110(6)	12.305(5)
<i>c</i> [Å]	18.2060(3)	16.2700(2)	14.8360(7)	18.7650(3)	16.763(1)	15.2310(7)	18.689(5)
α [°]	90	90	90	100.315(1)	90	84.644(2)	103.517(5)
β [°]	109.664(1)	100.830(5)	105.786(2)	91.037(1)	120.569(3)	80.594(2)	98.950(5)
γ [°]	90	90	90	109.245(1)	90	88.458(4)	99.066(5)
<i>V</i> [Å ³]	3454.33(8)	2809.37(7)	4276.4(3)	2745.62(6)	1386.1(1)	2217.0(2)	1984(1)
<i>Z</i>	4	4	4	4	2	2	2
ρ_{calc} [g cm ⁻³]	1.675	1.801	1.709	1.847	1.830	2.032	2.343
<i>F</i> (000)	1736	1488	2160	1488	744	1292	1304
crystal size [mm]	0.1 × 0.1 × 0.1	0.13 × 0.10 × 0.08	0.13 × 0.11 × 0.10	0.11 × 0.09 × 0.09	0.12 × 0.10 × 0.10	0.15 × 0.14 × 0.11	0.08 × 0.07 × 0.07
μ [mm ⁻¹]	4.32	5.29	3.86	5.41	5.36	7.26	11.51
rfins. collected	19237	33113	7871	22486	14475	17552	15603
rfins. unique	10080	8221	4707	15989	4044	10693	9094
rfins. obs. [<i>I</i> > 2 σ (<i>I</i>)]	6438	7046	3103	13309	2539	7974	6679
parameters	426	352	361	719	178	478	463
<i>R</i> indices	<i>R</i> ₁ = 0.040	<i>R</i> ₁ = 0.028	<i>R</i> ₁ = 0.052	<i>R</i> ₁ = 0.029	<i>R</i> ₁ = 0.048	<i>R</i> ₁ = 0.041	<i>R</i> ₁ = 0.045
[<i>I</i> > 2 σ (<i>I</i>)]	<i>wR</i> ₂ = 0.085	<i>wR</i> ₂ = 0.060	<i>wR</i> ₂ = 0.106	<i>wR</i> ₂ = 0.058	<i>wR</i> ₂ = 0.100	<i>wR</i> ₂ = 0.092	<i>wR</i> ₂ = 0.110

6-2CH₃OH·CH₃CN), CCDC-653222 (*cis*-7), CCDC-653223 (*cis*-8-2CHCl₃), CCDC-653224 (*cis*-9), CCDC-653225 (10-3CHCl₃), CCDC-653226 (11-2CH₂Cl₂), CCDC-653228 (*trans*-9) contain the supplementary crystallographic data for this paper that can be obtained free of charge from the Cambridge Crystallographic Data Centre via www.ccdc.cam.ac.uk/data_request/cif.

Photophysical experiments: All the experiments were carried out using spectrophotometric-grade solvents purchased from Merck, by using either air-equilibrated or argon-purged solutions. The solvents have been chosen to give a transparent matrix at 77 K. UV-Vis absorption spectra were recorded with a Perkin–Elmer λ 40 spectrophotometer, using quartz cells with a pathlength of 1.0 cm. Fluorescence spectra were performed with a Perkin–Elmer LS-50 or an Edinburgh FLS920 spectrofluorimeter, equipped with a Hamamatsu R928 phototube. Fluorescence lifetimes were measured by the above mentioned Edinburgh FLS920 spectrofluorimeter equipped with a TCC900 card for data acquisition in time-correlated single-photon counting experiments (0.5 ns time resolution) with a D₂ lamp. Measurements of emission spectra and lifetimes as a function of temperature were performed by inserting a quartz cell in a cryostat equipped with a temperature controller (model TC1) by Oxford Instruments. The estimated experimental errors are: ± 2 nm on the band maximum, 5% on the molar absorption coefficient, 5% on the fluorescence lifetime, 20% on the emission quantum yields. For solid samples, we made comparisons of emission quantum yields in the text; although the experimental error is rather large, we tried to minimize it by averaging multiple spectra without moving the sample for measurements in the presence or absence of vapors.

Acknowledgements

This work was supported by the Centre National de la Recherche Scientifique, the Ministère de l'Enseignement Supérieur et de la Recherche and the ANR (no. 06-BLAN-0410-01) in France and by MIUR (PRIN, "Sistemi supramolecolari per la conversione dell'energia luminosa") in Italy. We are grateful to Dr. N. Oberbeckmann-Winter for experimental help,

to Dr. A. DeCian (ULP Strasbourg) for the crystal structure data collection, and to Prof. R. Welter (ULP Strasbourg) for the refinement of the crystal structure of compound 7.

- [1] Z. Fei, P. J. Dyson, *Coord. Chem. Rev.* **2005**, *249*, 2056–2074.
- [2] See for example, a) P. Braunstein, *Chem. Rev.* **2006**, *106*, 134–159; b) P. Braunstein, F. Naud, *Angew. Chem.* **2001**, *113*, 702–722; *Angew. Chem. Int. Ed.* **2001**, *40*, 680–699; c) G. Helmchen, A. Pfaltz, *Acc. Chem. Res.* **2000**, *33*, 336–345; d) C. S. Slone, D. A. Weinberger, C. A. Mirkin, *Prog. Inorg. Chem.* **1999**, *48*, 233–350.
- [3] G. Margraf, R. Pattacini, A. Messaoudi, P. Braunstein, *Chem. Commun.* **2006**, 3098–3100.
- [4] H. L. Milton, M. V. Wheatley, A. M. Z. Slawin, J. D. Woollins, *Inorg. Chim. Acta* **2005**, *358*, 1393–1400.
- [5] Z. Garcia-Hernandez, A. Flores-Parra, J. M. Grevy, A. Ramos-Organillo, R. Contreras, *Polyhedron* **2006**, *25*, 1662–1672.
- [6] O. Kühn, B. Walfort, T. Ruffer, *Cryst. Growth Des.* **2006**, *6*, 366–368.
- [7] a) H. Nagashima, T. Sue, T. Oda, A. Kanemitsu, T. Matsumoto, Y. Motoyama, Y. Sunada, *Organometallics* **2006**, *25*, 1987–1994; b) Y. Sunada, T. Sue, T. Matsumoto, H. Nagashima, *J. Organomet. Chem.* **2006**, *691*, 3176–3182; c) D. Fenske, B. Maczek, K. Maczek, *Z. Anorg. Allg. Chem.* **1997**, *623*, 1113–1120; d) A. M. Baranger, R. G. Bergman, *J. Am. Chem. Soc.* **1994**, *116*, 3822–3835.
- [8] a) R. Uson, A. Laguna, M. Concepcion Gimeno, *J. Chem. Soc. Dalton Trans.* **1989**, 1883–1886; b) R. Uson, A. Laguna, M. Laguna, M. C. Gimeno, P. G. Jones, C. Fittschen, G. M. Sheldrick, *J. Chem. Soc., Chem. Commun.* **1986**, 509–510; c) J. Ellermann, W. Wend, *Nouv. J. Chim.* **1986**, *10*, 313–320; d) M. Knorr, unpublished results. e) P. A. Bella, O. Crespo, E. J. Fernandez, A. K. Fischer, P. G. Jones, A. Laguna, J. M. Lopez-de-Luzuriaga, M. Monge, *J. Chem. Soc. Dalton Trans.* **1999**, 4009–4017.
- [9] J. Powell, C. J. May, *J. Am. Chem. Soc.* **1982**, *104*, 2636–2637.
- [10] A. M. Z. Slawin, M. B. Smith, J. D. Woollins, *Chem. Commun.* **1996**, 2095–2096.
- [11] a) N. Oberbeckmann-Winter, P. Braunstein, R. Welter, *Organometallics* **2005**, *24*, 3149–3157; b) P. Braunstein, C. Frison, N. Ober-

- beckmann-Winter, X. Morise, A. Messaoudi, M. Bénard, M.-M. Rohmer, R. Welter, *Angew. Chem.* **2004**, *116*, 6246–6251; *Angew. Chem. Int. Ed.* **2004**, *43*, 6120–6125.
- [12] V. Balzani, V. Carassiti, *Photochemistry of Coordination Compounds*, Academic Press, London, New York, **1970**, p. 432 pp.
- [13] J. A. G. Williams, *Top. Curr. Chem.* **2007**, *281*, 205–268.
- [14] See e.g.: a) F. Barigelletti, A. Juris, V. Balzani, P. Belser, A. von Zelewsky, *J. Phys. Chem.* **1987**, *91*, 1095–1098; b) F. Barigelletti, P. Belser, A. von Zelewsky, A. Juris, V. Balzani, *J. Phys. Chem.* **1985**, *89*, 3680–3684.
- [15] a) P. J. Giordano, S. M. Fredericks, M. S. Wrighton, D. L. Morse, *J. Am. Chem. Soc.* **1978**, *100*, 2257–2259; b) R. J. Watts, J. S. Harrington, J. van Houten, *J. Am. Chem. Soc.* **1977**, *99*, 2179–2187.
- [16] M. Wrighton, D. L. Morse, *J. Am. Chem. Soc.* **1974**, *96*, 998–1003.
- [17] Emission quantum yields cannot be measured with our experimental equipment, but the data reported correspond to an average of multiple emission spectra recorded without moving the sample from the spectrofluorimeter. Therefore, the different emission intensities of the solid sample in different experimental conditions are meaningful within the large experimental error (20%).
- [18] For some examples, see: a) W. Lu, M. C. W. Chan, N. Zhu, C.-M. Che, Z. He, K.-Y. Wong, *Chem. Eur. J.* **2003**, *9*, 6155–6166; b) C. E. Buss, K. R. Mann, *J. Am. Chem. Soc.* **2002**, *124*, 1031–1039; c) S. M. Drew, D. E. Janzen, C. E. Buss, D. I. MacEwan, K. M. Dublin, K. R. Mann, *J. Am. Chem. Soc.* **2001**, *123*, 8414–8415.
- [19] F. R. Hartley, *The Chemistry of Platinum and Palladium*; Applied Science Publishers: London, **1973**.
- [20] R. Uson, A. Laguna, M. Laguna, *Inorg. Synth.* **1989**, *26*, 85.
- [21] a) A. Apfelbacher, P. Braunstein, L. Brissieux, R. Welter, *Dalton Trans.* **2003**, 1669–1674; b) P. Veya, C. Floriani, A. Chiesi-Villa, C. Guastini, A. Dedieu, F. Ingold, P. Braunstein, *Organometallics* **1993**, *12*, 4359–4367.
- [22] Bruker-Nonius, *Kappa CCD Reference Manual*, Nonius BV, The Netherlands, **1998**.
- [23] M Sheldrick; *SHELXL-97, Program for crystal structure refinement*; University of Göttingen: Germany, **1997**.

Received: July 14, 2007

Published online: October 15, 2007